processes

MDPI

Article

MicroscopicCharacteristics and Properties of Fe-Based Amorphous Alloy Compound Reinforced WC-Co-Based Coating via Plasma Spray Welding

Yan Xu [1,2], Yinfeng Wang [3], Yi Xu [3], Mingyong Li [3] and Zheng Hu [3,*]

1 China Research and Development Academy of Machinery Equipment, Beijing 100089, China; brenxuyan@gmail.com
2 School of Mechanical and Vehicle Engineering, Beijing Institute of Technology, Beijing 100081, China
3 Science and Technology on Vehicle Transmission Laboratory, China North Vehicle Research Institute, Beijing 100072, China; wangyf201@gmail.com (Y.W.); xuyitest201@gmail.com (Y.X.); mingyongli80@gmail.com (M.L.)
* Correspondence: huzhengnoveri@gmail.com

Abstract: Plasma spray welding, as one of the material surface strengthening techniques, has the advantages of low alloy material consumption, high mechanical properties and good coating compactness. Here, the Co alloy, WC and Fe-based amorphous alloy composite coating is prepared by the plasma spray welding method, and the coating characteristics are investigated. The results indicate that the coatings have a full metallurgical bond in the coating/substrate interface, and the powder composition influences the microstructures and properties of the coating. The hardness of coatings increases with the mass fraction of the Fe-based amorphous alloy. The spray welding layer has a much higher wear resistance compared with the carbon steel, and the Fe-20 exhibits a superior wear resistance when compared to others. The results indicate that the amorphous alloy powders are an effective additive to prepare the coating by plasma spray welding for improving the wear resistance of the coating.

Keywords: plasma spray welding; WC-Co coating; Fe-based amorphous alloy; microstructure and properties

Citation: Xu, Y.; Wang, Y.; Xu, Y.; Li, M.; Hu, Z. Microscopic Characteristics and Properties of Fe-Based Amorphous Alloy Compound Reinforced WC-Co-Based Coating via Plasma Spray Welding. *Processes* **2021**, *9*, 6. https://dx.doi.org/10.3390/pr9010006

Received: 16 November 2020
Accepted: 21 December 2020
Published: 22 December 2020

1. Introduction

The rapid development of the industry has led to increasingly higher requirements for the performance and service life of various mechanical parts [1–3]. Wear and corrosion are the prime reasons for material failure during use, which seriously affect the performance quality and service life of mechanical products [4–7]. Therefore, improving the wear resistance of the material surface is of great significance to reduce costs and save resources [8,9]. In order to improve the service life of structural steel in harsh environments, the plasma spray welding is an effective method to modify and strengthen the surface of the steel to form a new alloy coating to improve the wear and corrosion resistance of the material and reduce the production cost [10–13].

In the plasma spray welding technique, suitable alloy powders are selected according to the actual conditions and requirements of surface properties [14–16]. A spray welding layer of cobalt-based alloy has an excellent high temperature impact wear resistance and outstanding high temperature oxidative stability [17,18]. By optimizing the plasma spray welding process parameters, the quality of the spray welding layer has been improved, and different methods were proposed to reduce the spray welding layer cracks [19–22]. By adding different materials to the alloy powder to make composite materials, the structure and performance of the plasma spray welding layer are improved [23,24]. Especially in the aspects of hardness, wear resistance, corrosion resistance and oxidation resistance, the spray welding layer has achieved excellent results [25,26].

Numerous studies have shown that a transition metal-based amorphous alloy can be used directly as alloy powder or added to a nickel base, cobalt base, iron base and other self-fluxing alloyed powders owing to the high melting point, high hardness and good abrasive resistance. For example, $Fe_{45}Cr_{16}Mo_{18}C_{18}B_5$ amorphous coatings were deposited on the mild substrate by plasma spraying, and their corrosion in 3.5 wt.% NaCl solution was compared with those of the substrate and 316 stainless steel. The obtained results imply that the coating has a promising prospect for industrial applications [27]. Moreover, it has been reported that a WC-CoCr/35 wt.% amorphous Fe-based alloy composite coating was prepared by high velocity oxygen fuel spray, and, in comparison with the WC-CoCr coating, the WC-CoCr/35 wt.% amorphous Fe-based alloy composite coating exhibits excellent thermal stability and better corrosion resistance [28].

In this work, WC, Co and Fe-based alloy composite powders are selected to prepare a reinforced coating on the surface of 42CrMo steel using the plasma spray welding method. The Co-based amorphous alloy had excellent physicochemical properties, and the mechanical performance under high-temperature conditions was excellent [22,29]. The WC coating compounded with Co element has a high hardness value in a certain temperature range. At the same time, its impact resistance and toughness are very good, and the porosity of the coating is low, and it is combined with the substrate's high strength [3,30,31]. The influence and mechanism of the added Fe-based amorphous powder amount on the microstructure and properties of the spray welding layer are discussed. The results clearly show that the hardness of coatings increases with the mass fraction of the Fe-based amorphous alloy. The spray welding layer has a much higher wear resistance compared with the carbon steel, and the Fe-20 exhibits a superior wear resistance when compared to others.

2. Materials and Methods

2.1. Experimental Materials

42CrMo steel was adopted as the base material of plasma spray welding, and the 42CrMo chemical composition is shown in Table 1. WC (53–90 μm, 99.9 wt.%), Co alloy (53–165 μm) and Fe-based amorphous alloy (16–54 μm) are all products by Aidun Alloy Material Co., Ltd., Suzhou, China, and their chemical compositions are shown in Table 1.

Table 1. Chemical composition (wt.%) of the raw material.

Powder	C	Si	Mn	Cr	Mo	Ni	P	S	W	B	Fe	Co
42CrMo	0.45	0.37	0.8	1.2	0.25	0.03	0.03	0.03	–	–	rest	–
Co-Based Alloy	3.2	1.0	1.0	26.0	–	22.5	–	–	5.0	–	3.0	rest
Fe-Based Amorphous Alloy	1.7	1.8	–	4.0	–	7.5	–	–	–	3.0	rest	–

2.2. Experimental Methods

Firstly, Co alloy, WC and Fe-based amorphous alloy powders are mixed with ball-milling in a certain ratio (20%WC + Co + 5%Fe, 20%WC + Co + 10%Fe, 20%WC + Co + 15%Fe and 20%WC + Co + 20%Fe marked as Fe-5, Fe-10, Fe-15 and Fe-20). Secondly, the 42CrMo steel was cut into a sample of 30 × 50 × 10 mm using a wire cutting machine. Before plasma spray welding, the sample was polished with coarse sandpaper to remove the oxide layer and adjust the roughness, and then cleaned ultrasonically for 30 min in a bath of acetone to remove the rust, organic and fatty contaminants. Finally, a plasma spray welding was used on the 42CrMo steel surface to prepare the plasma welding layer, and the layer was about 23 × 35 mm. The spray welding layer was arc-shaped and the thickness about 2.7 mm. The technological parameters of the plasma spray welding are shown in Table 2.

Table 2. The plasma spray welding parameters.

Delivering Powder Gas Flow Rate (mL/min)	Plasma Gas Flow Rate (mL/min)	Feeding Voltage (V)	Standoff Distance (mm)	Powder Delivery Amount (g/min)	Current (A)	Bead Diameter (mm)
400	300	20	10	20	125	2

2.3. Detection and Analysis

Microstructure observations and a chemical analysis of the plasma spray welding layer were carried out by a field-emission scanning electron microscope (SEM, S-3000N, Hitachi, Tokyo, Japan) equipped with an energy-dispersive X-ray spectrometer (EDS). The phase composition of the sample was analyzed by the X-ray diffraction (XRD, D8 ADVANCE, BRUKER, Karlsruhe, Germany) and the parameters were set as follows: D/Max 2500PC, Cu Kα radiation, λ = 0.15418 nm, scan rate is 4°/min. Furthermore, the micro hardness of the sample was tested by adopting a micro-sclerometer (MH-3, Minks Testing Equipment Co., Ltd., Xi'an, China) for 10 s, with an applied load of 500g, and the test parameters were determined according to the composition of the material, the uniformity of the structure, the size and the surface roughness [32]. The wear resistance of the sample was tested by adopting an abrasive wear testing machine (ML-100, Jingcheng Testing Technology Co., Ltd., Jinan, China), with an applied load of 10 N. The stroke was 121.0 m and wear materials 600#SiC waterproof abrasive paper were used [33].

3. Result and Discussion

The results of the XRD analysis of the 20%WC + Co spray welding layer with different contents of Fe-based amorphous alloy are shown in Figure 1. It was found that the spray welding layer is mainly composed of carbides such as WC, Cr,Fe,Ni,Co(W,C) and $(Cr,Fe,Ni,Co)_3W_3C$, as well as the alloy phase of Cr, Fe, Ni and Co. Cr,Fe,Ni,Co(W,C) is an fcc solid solution of W and C in the metal lattice with a larger lattice parameter, whereas $(Cr,Fe,Ni,Co)_3W_3C$ is a metastable sub-stoichiometric ternary carbide called η-phase (M_6C, where M = metal). Since the Cr, Fe and Co elements have a strong affinity with the C element, they could form carbides easily. The carbides have both a high hardness and excellent wear resistance and can be used as a hard phase supporting matrix, which can greatly improve the hardness and wear resistance of the spray welding layer [34]. Figure 1b shows the XRD analysis results of Fe-20. Compared to Fe-5, a much harder phase was formed on the surface of the substrate. This can be attributed to the fact that an increase of the Fe content would generate a harder phase in the spray welding process, which is conducive to comprehensively improving the hardness, wear resistance and other mechanical properties of the spray-welding layer.

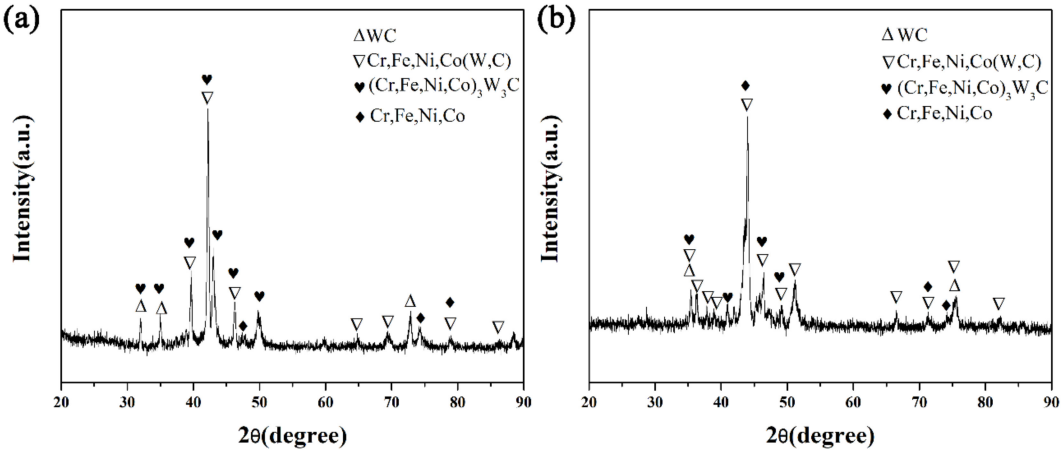

Figure 1. XRD patterns of the coatings with different Fe-based amorphous alloy contents. (**a**) 5%, (**b**) 20%.

The typical surface morphology of the coatings with a different Fe-based amorphous alloy content are characterized by SEM, as shown in Figure 2. The Fe-based amorphous alloy content of 5% is shown in Figure 2a, where it can be clearly seen that the white phase is the carbide phase, which is the main existing style of carbide particles in the spray welding layer, and the dark gray phase is mainly the matrix solid solution phase. As shown in Figure 2, the white carbide phase mainly exists in the form of regular dendrites in the spray welding layer. As the Fe-based amorphous alloy content increases, the number and size of dendritic solidification structures also increase, as shown in Figure 2b. It is worth noting that few WC particles are observed in the coating surface, which is due to the different melting points and densities of WC and the metal phase during the rapid cooling rate in the plasma spray welding process. The WC melting point, which is the highest compared to that of the metal phase, is about 2870 °C. During the process of coating formation, the metal phase is melted into liquid owing to the higher hot plasma energy, while the WC powder is hard to melt. Then, the WC powder with a high density would sink down inward because of gravity. In order to confirm the main phase in the coating surface, the elemental composition of the surface of the spray welding layer was analyzed, and the results of points 1–4 are shown in Table 3. It can be clearly seen that points 1 and 3 have the same elements, including C, Si, Cr, Fe, Co, W and Ni. And so do points 2 and 4, compared with points 1 and 3, which lack the Si element. The results indicate that the white area's chemical component in the dendritic crystal is composed of WC and that the dendritic crystal is mainly composed of $(Cr,Fe,Ni,Co)_3W_3C$, while the matrix's solid solution phase is mainly composed of Cr,Fe,Co,Ni(C). Moreover, it was found that the Fe, Cr, Ni and Co elements in the carbide phase are significantly less than that in the matrix, while the W elements in the carbide phase are more numerous than that in the matrix.

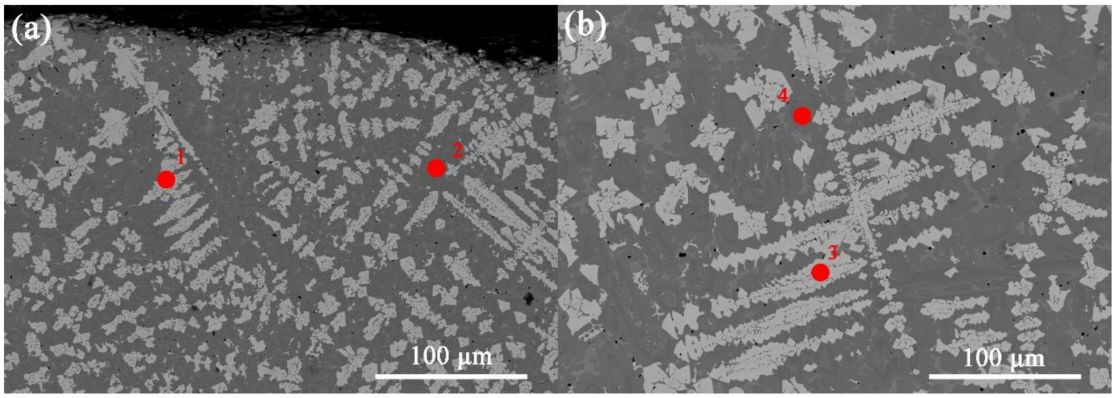

Figure 2. Surface SEM images of different coatings: (**a**) Fe-5 and (**b**) Fe-20.

Table 3. Chemical composition (at %) of the surface of the spray welding layer.

	C	Si	Cr	Fe	Co	W	Ni
1	16.96	1.76	15.69	7.73	21.22	25.56	11.08
2	15.07	–	22.42	8.98	36.09	2.21	15.23
3	19.21	2.93	14.94	9.59	20.79	22.96	9.58
4	17.74	–	19.7	10.61	35.15	2.05	14.75

Figure 3 shows the SEM of the cross-section of the samples' spray welding layer. The result shows that the coating has a dense microstructure and the thermal plasma beam can ensure metallurgical bonding between the coating and the 42CrMo steel. As shown in Figure 3a,e, it was found that the WC particles are not evenly distributed. There are few WC particles in the surface zone of coating, while the WC particles are concentrated in the fusion zone nearing the steel surface. The microstructures of the surface zone are shown in Figure 3b,f. It is clear that most of the carbide phases are dendritic structures,

some of which are irregular in shape and distributed among the dendritic structures. Figure 3c,g show the microstructures of the middle zone. Compared with the surface zone, the irregular WC particles in the middle zone increase and the carbide phases with dendritic structure decrease. Figure 3d,h shows the structure of the fusion zone. It can be clearly seen that there are plenty of WC particles with a surrounded dendritic structure. This is due to the plasma spray welding process. The melting point of WC is too high, and the WC exists in a semi-melted form in the liquid metal. The semi-melted WC particles can be used as nucleation particles in the liquid phase solidification process to promote non-uniform nucleation, causing the local segregation of alloy components and promoting the growth of nucleation particles in the form of dendrites during the solidification of the liquid phase metal [35]. In a certain crystal grain range, the hardness decreases with the increase of WC crystal grains. This is due to the small size effect of fine grain WC, large surface energy, effective flow for liquid phase diffusion during the spray welding process, uniform grain growth and high densification, which improves the mechanical properties [36,37]. As shown in Figure 3c,d, it was found that the crystal grain of WC is bigger than tin Figure 3g,h indicating that the properties of Fe-20 are superior to those of Fe-5.When the grains have an uneven distribution and an irregular growth, the mechanical properties of the coating are reduced. It can be seen that the grains' uneven distribution in Fe-5 and Fe-20 affect the performance of the coating. Besides, the shape of the carbide phase is significantly different from the difference in local alloy composition carbides and temperature gradient. Furthermore, the EDS analysis results of the middle zone in Fe-20 are shown in Figure 3i–l. It is obvious that the W elements are mainly distributed in the WC phase and the carbide phase, while the Fe, Cr, Ni and Co elements in the matrix are more numerous than the carbide phase. Several points are selected to further explore the chemical composition in the fusion zone, and the results of the electronic probe are shown in Table 4. It was found that point 1 only contains the C and W elements, indicating that the place of the point is WC. Points 2 and 3 contain the same elements, including C, Si, Cr, Fe, Co, W and Ni. It is confirmed that the WC particles are surrounded by a carbide phase with a dendritic structure. However, the distribution of elements in the carbide phase is quite different at different positions. The carbide phase near the WC phase has more W elements than those away from the WC phase. The reason is that, during the plasma spray welding process, WC gradually melts and releases W elements which would induce a high concentration of W around the WC particles, while these W elements would form a $(Cr,Fe,Ni,Co)_3W_3C$ phase. In addition, the results of EDS component analysis show that the Fe content in point 3 is significantly higher than that in point 2. This is because the melting of the sub-matrix will cause the elements in the matrix to enter the molten pool. As a result, the Fe content is much higher, while the other elements in the fusion zone are diluted.

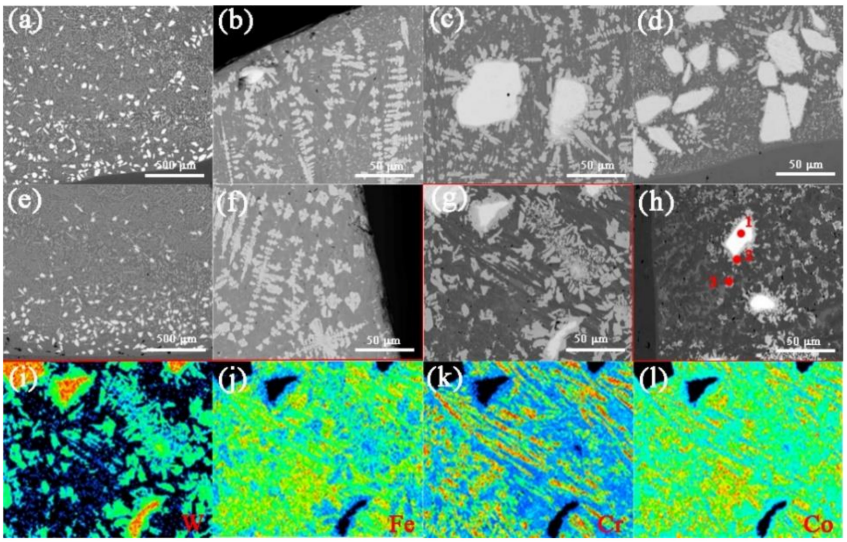

Figure 3. SEM images of (**a**–**d**) the cross-section of the Fe-5 coating, (**e**–**h**) SEM images of the cross-section of the Fe-20 coating and (**i**–**l**) EDS images of the middle zone in the Fe-20 coating.

Table 4. Chemical composition (at %) of the points in the fusion zone.

	C	Si	Cr	Fe	Co	W	Ni
1	45.62	–	–	–	–	54.38	–
2	17.31	2.03	14.24	8.29	19.4	28.52	10.21
3	15.25	1.26	12.02	26.59	18.71	17.69	8.48

The influence of the contents of Fe-based amorphous alloys on the binding quality, microhardness and wear resistance property of the spray welding layer was further studied. Figure 4 shows the binding quality of the coating to the substrate. It can be seen that when the Fe-based amorphous alloy content is 20%, the spray welding layer can be well combined with the substrate, and when the Fe-based amorphous alloy content is relatively lower, the spray welding layer cannot form an excellent cladding with the substrate. When the content of the Fe-based amorphous alloy is 5%, the spray welding current is relatively too large to meet the requirement of the spray welding, so that the spray welding layer cannot be well fused with the substrate, resulting in spray welding defects. The microhardness distribution ranging from substrate to coating is shown in Figure 5a. It can be clearly seen that the hardness of the 42CrMo steel substrate is about 320 HV and the hardness of the spray welding layer is about 650–750 HV. The microhardness of the coating is about two times higher than that of the substrate for each coating. The microhardness of the spray welding layer fluctuates slowly, which may be caused by the difference in the size and quantity distribution of the hard phase. It was found that the hardness gradient in the bonding domain is large, which is a typical characteristic of the hardness distribution of the spray welding layer. This is the result of the sprayed liquid alloy and the matrix, which diffuse and penetrate each other, and the C element in the alloy power plays a solid solution strengthening effect [38,39]. Besides, as the content of Fe-based amorphous alloys increases, the microhardness of the spray welding layer increases, and has a great relationship with the microstructure. The increase of the carbide phase in the spray welding layer and the distribution lead to an increase in the hardness of the spray welding layer [40–42].

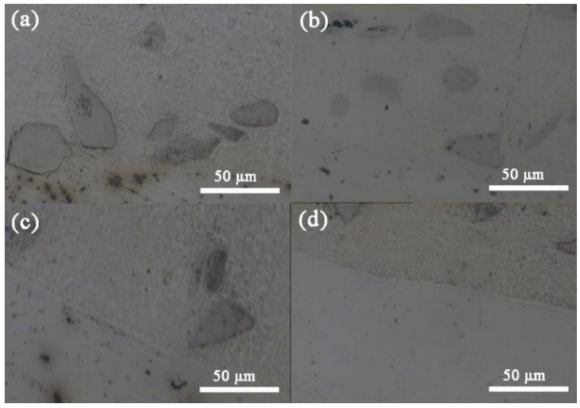

Figure 4. The different contents of the Fe-based amorphous alloy of the binding quality to the substrate (**a**) Fe-5 (**b**) Fe-10 (**c**) Fe-15 (**d**) Fe-20.

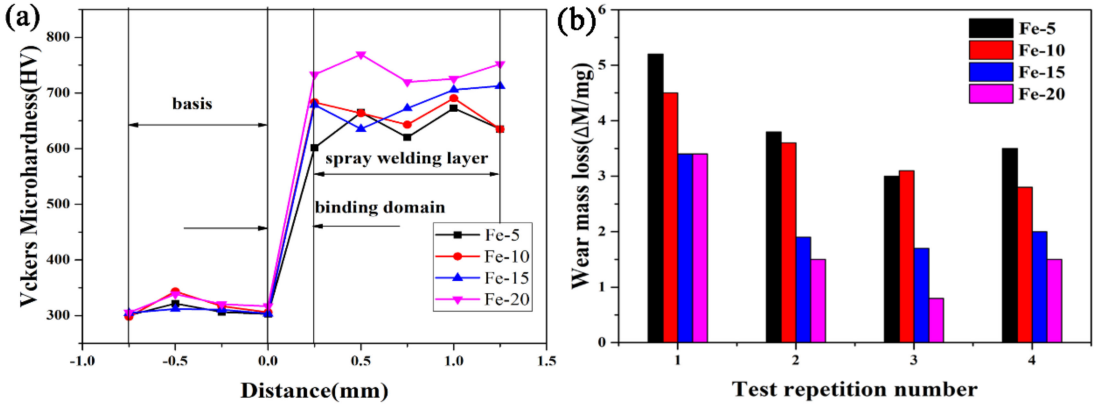

Figure 5. The influence of the Fe-based amorphous alloy content on the mechanical properties of the plasma spray welding layer: (**a**) microhardness and (**b**) wear mass loss.

Wear mass loss is an important factor in characterizing the wear resistance of a material. The results of the wear mass loss are shown in Figure 5b. The wear mass loss of the spray welding layer of Fe-5, Fe-10 and Fe-15 is more than that of Fe-20. The smaller the wear loss rate, the better the wear resistance of the spray welding layer. When the amount of the Fe-based amorphous alloy added is 20%, the spray welding layer has better wear resistance. When the amount of the Fe-based amorphous alloy added is 5–15%, the microhardness and wear resistance are reduced. This is because when a small amount of Fe-based amorphous alloy is added, it can only play a solid solution strengthening effect [33,43]. Additionally, as shown in Figure 4b, the wear mass loss of the following three frictions and wear experiments is relatively balanced, while the wear mass loss of the first time is relatively high. This is because the surface is the outermost in the first wear experiment, which has a lower degree of bonding than the inside.

To further explore the influence of different Fe-based amorphous alloys on the wear resistance of the spray welding layer, frication and wear experiments were carried out on the samples. The morphologies of the worn surfaces of the coatings are shown in Figure 6. Figure 6a–c shows the SEM images of Fe-5, Fe-10 and Fe-15. Deep furrows and scratches are clearly visible on the sample surface, caused by the splashing and agglomeration of Fe-based amorphous alloys. The powder fails to effectively bond with the matrix when it is melted, resulting in a decrease in the Fe-based amorphous alloys content in the spray welding layer and an increase in the austenite phase content. The spray welding layer becomes soft, causing the furrows to deepen. Figure 6d shows the wear morphology of the Fe-20 spray welding layer. Fewer scratches and spalling pits were found, and there are almost no deep furrows in the spray welding layer's wear scars. Meanwhile, more hard

phases are scattered in the spray welding layer. The structure is small and uniform, and the hardness and toughness reach a good level. Therefore, the spray welding layer has a better wear resistance.

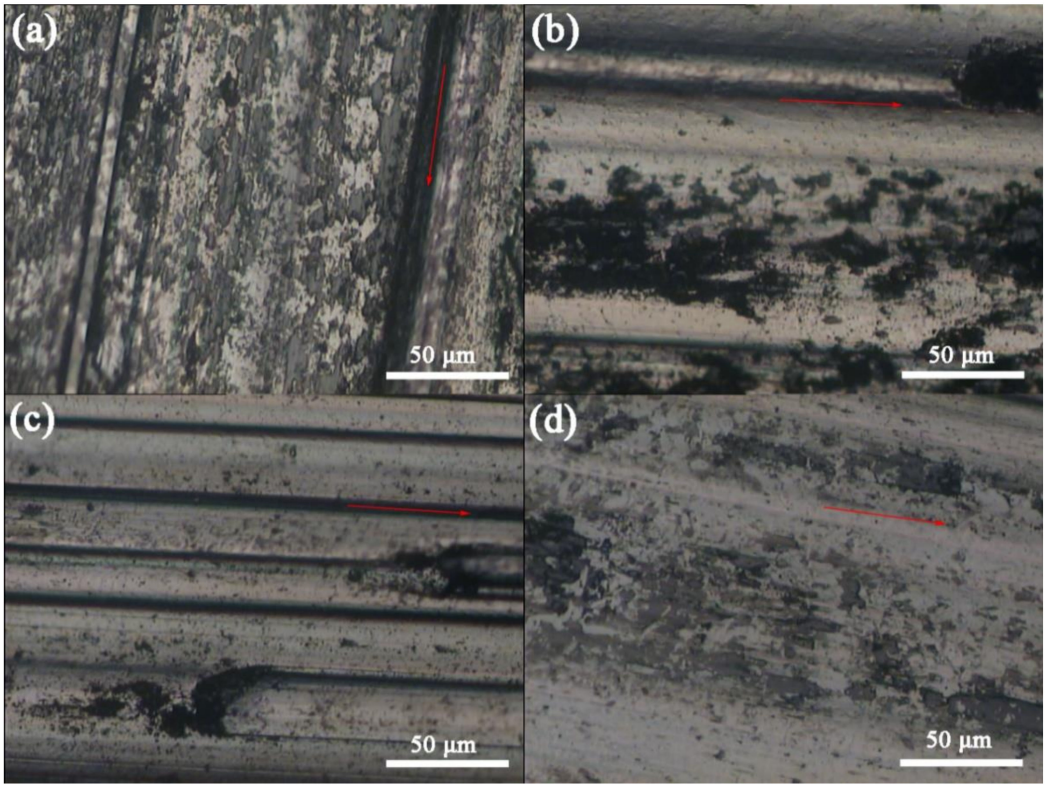

Figure 6. The morphologies of worn coatings: (**a**) Fe-5, (**b**) Fe-10, (**c**) Fe-15 and (**d**) Fe-20.

4. Conclusions

In summary, Fe-based amorphous alloy reinforced WC-Co-based coating was prepared on 42CrMo steel by plasma spray welding. The results indicate that the coatings have a full metallurgical bond in coating/substrate interface and the powder composition influences the microstructures and properties of the coating. The main components of the coating are WC, Cr,Fe,Ni,Co(W,C), $(Cr,Fe,Ni,Co)_3W_3C$ and the alloy phase of Cr, Fe, Ni and Co. Experimental result shows that the interface between the spray welding layer and matrix has a large amount of WC, and there is a gradient distribution of WC from internal to external in the cross section. The spray welding layer would enhance the hardness and wear resistance of the 42CrMo steel. The hardness of the coatings increased with the mass fraction of the Fe-based amorphous alloy. The spray welding layer has a much higher wear resistance compared with the carbon steel, and Fe-20 exhibits a superior wear resistance when compared to others.

Author Contributions: Data curation, Y.W. and Y.X. (Yi Xu); formal analysis, M.L.; investigation, Y.X. (Yan Xu) and Y.X. (Yi Xu); project administration, Y.X. (Yi Xu) and Z.H. All authors have read and agreed to the published version of the manuscript.

Funding: This research was funded by the Innovation Program (237099000000170004).

Acknowledgments: The authors would like to acknowledge the financial supports of the Innovation Program (237099000000170004).

Conflicts of Interest: The authors declare no conflict of interest.

References

1. Singh, G.; Kumar, S.; Kumar, R. Comparative study of hot corrosion behavior of thermal sprayed alumina and titanium oxide reinforced alumina coatings on boiler steel. *Mater. Res. Express* **2020**, *7*, 26527. [CrossRef]
2. Dong, T.S.; Zheng, X.D.; Li, Y.L.; Li, G.L.; Zhou, X.K.; Wang, H.D. Microstructure and Wear Resistance of FeCrBSi Plasma-Sprayed Coating Remelted by Gas Tungsten Arc Welding Process. *J. Mater. Eng. Perform.* **2018**, *27*, 4069–4076.
3. Jiang, Q.; Tian, Y.; Shu, F.; Zhao, H.; Sun, Y.; He, W.; Xu, B. Strengthening mechanism and properties of Co–WC composite coatings deposited by plasma-transferred arc welding. *Micro Nano Lett.* **2019**, *14*, 717–720. [CrossRef]
4. Zhang, Y.; Chi, Q.; Chang, L.; Dong, Y.; Cai, P.; Pan, Y.; Gong, M.; Huang, J.; Li, J.; He, A.; et al. Novel Fe-based amorphous compound powder cores with enhanced DC bias performance by adding FeCo alloy powder. *J. Magn. Magn. Mater.* **2020**, *507*, 166840. [CrossRef]
5. Leal, E.; Gomes, U.; Alves, S.; Costa, F. The influence of powder preparation condition on densification and microstructural properties of WC-Co- Al2O3 cermets. *Int. J. Refract. Met. Hard Mater.* **2020**, *92*, 105275. [CrossRef]
6. Hu, L.; Huang, J.; Liu, C.; Liu, X.; Hou, D.; Xu, C.; Zhao, Y. Effects of coupling between the laser plasma and two arcs on metal transfer in CO2 laser double-wire MIG hybrid welding. *Opt. Laser Technol.* **2018**, *105*, 152–161. [CrossRef]
7. Kawase, M.; Ido, A.; Morinaga, M. Development of $SiO_2/TiO_2/Al_2O_3$-based/TiO_2 coating for preventing sulfide corrosion in thermal power plant boilers. *Appl. Therm. Eng.* **2019**, *153*, 242–249. [CrossRef]
8. Zhang, S.; Sun, J.; Zhu, M.; Zhang, L.; Nie, P.; Li, Z. Effects of shielding gases on process stability of 10CrNi3MoV steel in hybrid laser-arc welding. *J. Mater. Process. Technol.* **2019**, *270*, 37–46. [CrossRef]
9. Wang, Q.; Zhou, Y.; Zhou, J.; Zhang, G. Microstructure and properties of PTA sprayed 310/WC composite coating. *Mater. Res. Express* **2019**, *6*, 66561. [CrossRef]
10. Liang, X.; Liu, Z.; Wang, B. Multi-pattern failure modes and wear mechanisms of WC-Co tools in dry turning Ti–6Al–4V. *Ceram. Int.* **2020**, *46*, 24512–24525. [CrossRef]
11. Mironchuk, B.; Abrosimova, G.E.; Bozhko, S.; Drozdenko, A.; Postnova, E.; Aronin, A. Phase transformation and surface morphology of amorphous alloys after high pressure torsion. *Mater. Lett.* **2020**, *273*, 127941. [CrossRef]
12. Ma, D.-D.; Xue, Y.-P.; Gao, J.; Ma, Y.; Yu, S.-W.; Wang, Y.-S.; Xue, C.; Hei, H.-J.; Tang, B. Effect of Ta diffusion layer on the adhesion properties of diamond coating on WC-Co substrate. *Appl. Surf. Sci.* **2020**, *527*, 146727. [CrossRef]
13. Methong, T.; Shigeta, M.; Tanaka, M.; Ikeda, R.; Matsushita, M.; Poopat, B. Visualization of gas metal arc welding on globular to spray transition current. *Sci. Technol. Weld. Join.* **2017**, *23*, 87–94. [CrossRef]
14. Staia, M.; Mejias, A.; La Barbera, J.G.; Puchi-Cabrera, E.; Villalobos-Gutierrez, C.; Santana, Y.Y.; Montagne, A.; Iost, A.; Rodriguez, M.A. Mechanical properties of WC/Co-CNT HVOF sprayed coatings. *Surf. Eng.* **2018**, *36*, 1156–1164. [CrossRef]
15. Yan, W.; Qin, H.; Qiang, X.; Zhong, X. Microstructures and Wear Behavior of Ni-based Spray-welding Coating on Pure Titanium TA1 Substrate. *Rare Metal. Mat. Eng.* **2018**, *47*, 910–914.
16. Maslarevic, A.; Bakic, G.M.; Djukic, M.B.; Rajicic, B.; Maksimovic, V.; Pavkov, V. Microstructure and Wear Behavior of MMC Coatings Deposited by Plasma Transferred Arc Welding and Thermal Flame Spraying Processes. *Trans. Indian Inst. Met.* **2020**, *73*, 259–271. [CrossRef]
17. Kendzia, B.; Koppisch, D.; Van Gelder, R.; Gabriel, S.; Zschiesche, W.; Behrens, T.; Brüning, T.; Pesch, B. Modelling of exposure to respirable and inhalable welding fumes at German workplaces. *J. Occup. Environ. Hyg.* **2019**, *16*, 400–409. [CrossRef]
18. Yu, J.; Wang, B.; Zhang, H.; Wang, Q.; Wei, L.; Chen, P.; He, P.; Feng, J. Characteristics of Magnetic Field Assisting Plasma GMAW-P The effect of the magnetic field intensity on droplet transition in plasma-GMAW-P hybrid welding was studied. *Weld J.* **2020**, *99*, S25–S38. [CrossRef]
19. Bayar, I.; Ulutan, M. Surface modification of atmospheric plasma sprayed cermet coatings by plasma transferred arc method. *Trans. IMF* **2019**, *97*, 298–304. [CrossRef]
20. Baiamonte, L.; Tului, M.; Bartuli, C.; Marini, D.; Marino, A.L.; Menchetti, F.; Pileggi, R.; Pulci, G.; Marra, F. Tribological and high-temperature mechanical characterization of cold sprayed and PTA-deposited Stellite coatings. *Surf. Coatings Technol.* **2019**, *371*, 322–332. [CrossRef]
21. Huang, E.-W.; Hung, G.-Y.; Lee, S.Y.; Jain, J.; Chang, K.-P.; Chou, J.J.; Yang, W.-C.; Liaw, P.K. Mechanical and Magnetic Properties of the High-Entropy Alloys for Combinatorial Approaches. *Crystals* **2020**, *10*, 200. [CrossRef]
22. Zhao, J.; Gao, Q.; Wang, H.; Shu, F.; Zhao, H.; He, W.; Yu, Z. Microstructure and mechanical properties of Co-based alloy coatings fabricated by laser cladding and plasma arc spray welding. *J. Alloys Compd.* **2019**, *785*, 846–854. [CrossRef]
23. Dong, S.; Jiang, F.; Xu, B.; Chen, S. Influence of Polarity Arrangement of Inter-Wire Arc on Droplet Transfer in Cross-Coupling Arc Welding. *Materials* **2019**, *12*, 3985. [CrossRef] [PubMed]
24. Zhao, Y.; Chung, H. Numerical simulation of the transition of metal transfer from globular to spray mode in gas metal arc welding using phase field method. *J. Mater. Process. Technol.* **2018**, *251*, 251–261. [CrossRef]
25. Zhu, R.; Gao, W. Wear-resistance Performance of Spray-welding Coating by Plasma Weld-surfacing. *J. Wuhan Univ. Technol. Sci. Ed.* **2018**, *33*, 414–418. [CrossRef]
26. Shi, B.; Huang, S.; Zhu, P.; Xu, C.; Guo, P.; Fu, Y. In-situ TiN reinforced composite coatings prepared by plasma spray welding on Ti6Al4V. *Mater. Lett.* **2020**, *276*, 128093. [CrossRef]
27. Chu, Z.; Deng, W.; Zheng, X.; Zhou, Y.; Zhang, C.; Xu, J.; Gao, L. Corrosion Mechanism of Plasma-Sprayed Fe-Based Amorphous Coatings with High Corrosion Resistance. *J. Therm. Spray Technol.* **2020**, *29*, 1111–1118. [CrossRef]

28. Xu, L.P.; Song, J.B.; Deng, C.G.; Liu, M.; Zhou, K.S. Microstructure and Properties of WC-based Coating Reinforced by Fe-based Amorphous Alloys. *Rare Metal Mat. Eng.* **2020**, *49*, 1546–1552.
29. Kim, W.R.; Heo, S.; Kim, J.-H.; Park, I.-W.; Chung, W. Multi-Functional Cr-Al-Ti-Si-N Nanocomposite Films Deposited on WC-Co Substrate for Cutting Tools. *J. Nanosci. Nanotechnol.* **2020**, *20*, 4390–4393. [CrossRef]
30. Zhang, L.; Yue, F.; Li, S.F.; Yang, Y.F. Utilizing the autocatalysis of Co to prepare low-cost WC-Co powder for high-performance atmospheric plasma spraying. *J. Am. Ceram. Soc.* **2020**, *103*, 6690–6699. [CrossRef]
31. Hu, M.; Tang, J.; Chen, X.-G.; Ye, N.; Zhao, X.-Y.; Xu, M.-M. Microstructure and properties of WC-12Co composite coatings prepared by laser cladding. *Trans. Nonferrous Met. Soc. China* **2020**, *30*, 1017–1030. [CrossRef]
32. Mostajeran, A.; Shoja-Razavi, R.; Hadi, M.; Erfanmanesh, M.; Barekat, M.; Firouzabadi, M.S. Evaluation of the mechanical properties of WC-FeAl composite coating fabricated by laser cladding method. *Int. J. Refract. Met. Hard Mater.* **2020**, *88*, 105199. [CrossRef]
33. Huang, F.; Xu, H.; Liu, W.; Zheng, S. Microscopic characteristics and properties of titaniferous compound reinforced nickel-based wear-resisting layer via in situ precipitation of plasma spray welding. *Ceram. Int.* **2018**, *44*, 7088–7097. [CrossRef]
34. Boukantar, A.-R.; Djerdjare, B.; Guiberteau, F.; Ortiz, A.L. Spark plasma sinterability and dry sliding-wear resistance of WC densified with Co, Co+Ni, and Co+Ni+Cr. *Int. J. Refract. Met. Hard Mater.* **2020**, *92*, 105280. [CrossRef]
35. Hua, N.; Zhang, X.; Liao, Z.; Hong, X.; Guo, Q.; Huang, Y.; Ye, X.; Chen, W.; Zhang, T.; Jin, X.; et al. Dry wear behavior and mechanism of a Fe-based bulk metallic glass: Description by Hertzian contact calculation and finite-element method simulation. *J. Non-Cryst. Solids* **2020**, *543*, 120065. [CrossRef]
36. Itagaki, H.; Yachi, T.; Ogiso, H.; Sato, H.; Yamashita, Y.; Yasuoka, J.; Funada, Y. DC Arc Plasma Treatment for Defect Reduction in WC-Co Granulated Powder. *Metals* **2020**, *10*, 975. [CrossRef]
37. Fu, W.; Chen, Q.-Y.; Yang, C.; Yi, D.-L.; Yao, H.-L.; Wang, H.-T.; Ji, G.-C.; Wang, F. Microstructure and properties of high velocity oxygen fuel sprayed (WC-Co)-Ni coatings. *Ceram. Int.* **2020**, *46*, 14940–14948. [CrossRef]
38. Li, C.; Wang, H.; Ding, J.; Wang, S.; Li, J.; Kou, S. Effects of heat treatment on HVOF-sprayed Fe-based amorphous coatings. *Surf. Eng.* **2020**. [CrossRef]
39. Derakhshandeh, M.; Eshraghi, M.; Jam, A.; Rajaei, H.; Fazili, A. Comparative studies on corrosion and tribological performance of multilayer hard coatings grown on WC-Co hardmetals. *Int. J. Refract. Met. Hard Mater.* **2020**, *92*, 105339. [CrossRef]
40. Ning, W.; Zhai, H.; Xiao, R.; He, D.; Liang, G.; Wu, Y.; Li, W.; Li, X. The Corrosion Resistance Mechanism of Fe-Based Amorphous Coatings Synthesised by Detonation Gun Spraying. *J. Mater. Eng. Perform.* **2020**, *29*, 3921–3929. [CrossRef]
41. Ogino, Y.; Hirata, Y.; Asai, S. Discussion of the Effect of Shielding Gas and Conductivity of Vapor Core on Metal Transfer Phenomena in Gas Metal Arc Welding by Numerical Simulation. *Plasma Chem. Plasma Process.* **2020**, *40*, 1109–1126. [CrossRef]
42. Shi, B.; Huang, S.; Zhu, P.; Xu, C.; Zhang, T. Microstructure and Wear Behavior of In-Situ NbC Reinforced Composite Coatings. *Materials* **2020**, *13*, 3459. [CrossRef] [PubMed]
43. Stummer, M.; Stütz, M.; Aumayr, A.; Enzinger, N. Electron beam welding of copper using plasma spraying for filler metal deposition. *Weld. World* **2018**, *62*, 1341–1350. [CrossRef]